UNIVERSIDAD SAN FRANCISCO DE QUITO USFQ

Colegio de Ciencias e Ingenierías

Optical Vortices and Interferometry in the Nematic Liquid Crystal MBBA

Proyecto de investigación

Juan Pablo Yunda Díaz

Licenciatura en Física

Trabajo de titulación presentado como requisito
para la obtención del título de Licenciado en Física

Quito, 29 de noviembre de 2017

UNIVERSIDAD SAN FRANCISCO DE QUITO USFQ
COLEGIO DE CIENCIAS E INGENIERÍAS

HOJA DE CALIFICACIÓN
DE TRABAJO DE TITULACIÓN

Optical Vortices and Interferometry in the Nematic Liquid Crystal MBBA

Juan Pablo Yunda Díaz

Calificación:

Nombre del profesor, Título académico: Melissa Infusino, Ph.D.

Firma del profesor: _____

Quito, 29 de noviembre de 2017

DERECHOS DE AUTOR

Por medio del presente documento certifico que he leído todas las Políticas y Manuales de la Universidad San Francisco de Quito USFQ, incluyendo la Política de Propiedad Intelectual USFQ, y estoy de acuerdo con su contenido, por lo que los derechos de propiedad intelectual del presente trabajo quedan sujetos a lo dispuesto en esas Políticas.

Asimismo, autorizo a la USFQ para que realice la digitalización y publicación de este trabajo en el repositorio virtual, de conformidad a lo dispuesto en el Art. 144 de la Ley Orgánica de Educación Superior.

Firma del estudiante: _____

Nombres y apellidos: Juan Pablo Yunda Díaz

Código: 00112238

Cédula de identidad: 172035000-6

Lugar y fecha: Quito, 29 de noviembre de 2017

Resumen

En este trabajo se muestra el comportamiento de la luz cuando pasa por un defecto localizado en una red de difracción formada con el cristal líquido nemático MBBA. Se encontró que el MBBA produce un reordenamiento bastante estable para un voltaje aplicado de $V = 6.81\,[V]$, en el cual se observó franjas paralelas con algunos defectos tipo "fork", con carga topológica singular. Las franjas paralelas son conocidas como "Dominios de Williams" y tienen una periodicidad uniforme igual al espesor de la celda que contiene al cristal líquido. La difracción es producida porque el MBBA es un material birrefringente y se produce una modulación en el indice de refracción debido a inestabilidades electro-convectivas. Diferentes experimentos de interferometría permitieron encontrar el momento angular de los rayos difractados por este tipo de dislocaciones de borde. Para esto se usó un rayo de referencia con una onda plana y otro con una onda esférica, obteniendo patrones de interferencia que satisfacen el comportamiento teórico de la luz a través de vórtices ópticos de carga topológica singular. Inicialmente se estudió el comportamiento de los primeros órdenes difractados, pero este estudio se puede extender a los órdenes superiores. Sin interferometría, se observa que los rayos difractados muestran vórtices ópticos, es decir su centro es oscuro, similar a un anillo. Los patrones de interferencia aportan información visual de la fase, debido a la interferencia constructiva de la luz.

Palabras clave: Cristal líquido, nemático, Dominios de Williams, birrefringencia, difracción, interferometría, vórtices ópticos, defectos ópticos.

Abstract

In this work we show the behavior of light when it impinges through a localized defect in a diffraction made by the nematic liquid crystal MBBA. We found that MBBA creates a very stable reordering for an applied voltage of $V = 6.81\,[V]$, for which we observed parallel fringes with several "fork" shaped defects, with single topological charge. This fringes are known as "Williams Domains" and have a uniform periodicity equal to the thickness of the cell containing the liquid crystal. Diffraction is produced because MBBA is a birefringent material and there is a modulation in the refraction index given by electro-convective instabilities. Different experiments of interferometry allowed us to find the angular momentum of the light beams diffracted by this kind of edge dislocation. For this purpose we used two reference beams, one with a plane wave and the other one with a spherical wave, getting interference patterns that fulfill the theoretical behavior of light after going through optical vortices with single topological charge. Initially the first order diffraction was studied, but this work could be extended for higher orders. Without interferometry, optical vortices are observed in the diffracted light beams, which implies that its center is dark, similar to a ring. The interference patterns give visual information of the phase, because of the constructive interference of light.

Key words: Liquid crystal, nematic, Williams Domains, birefringence, diffraction, interferometry, optical vortices, optical defects.

Agradecimientos

Quiero agradecer a mi familia y amigos porque siempre han estado pendientes de mí.

Agradezco a la Universidad San Francisco por haberme permitido estudiar con el programa de becas. Igualmente por el programa de intercambio en la Universidad de Illinois, donde pasé un año muy productivo y conocí a buenos amigos. Quiero agradecer al Departamento de Física de la USFQ por innovar constantemente y traer profesores extranjeros de excelente nivel.

Agradezco también a Melissa Infusino por haberme ayudado desde el inicio de este trabajo, haberme ayudado a conseguir una pasantía en Italia y haberme hospedado con su familia. También agradezco al CNR (Centro Nationale de la Ricerca) de Italia por permitirme utilizar los laboratorios de la Universidad de la Calabria y ayudarme a cubrir gastos relacionados con este trabajo.

Dedicado a John Bardeen, por el transistor. Transistor que dio origen a computadoras

que nos permiten investigar con rapidez, incluso cometiendo errores.

Contents

List of Figures

1 Introduction

Generally described as the intermediate state between a solid and liquid state, liquid crystals have the property of changing their organization when some external physical factor is changed. They are divided in two subcategories: thermotropic liquid crystals where the organization and the degree of order is regulated by temperature and lyotropic liquid crystals where their organization is regulated by changing the molecule concentration using a solvent. Most of the organic compounds are known to be in a liquid crystal state, because these molecules are found to be geometrically anisotropic, like rodes or disks. This geometrical property is needed for mesomorphism of liquid crystals [2]. Some liquid crystals have some mesophases (intermediate phases) before they are transformed into the isotropic liquid phase. The liquid crystal could be in three mesophases: nematic, smetic and cholesteric. Liquid crystals have several applications in optical physics in each of this mesophases. In this work, I focused on the study of the nematic phase of MBBA.

1.1 Nematic Liquid Crystal

Nematics are characterized for having its molecules in a partially ordered pattern, where all the molecules are mostly parallel to a preferred axis (long axis) which is known as the molecular director, $\vec{n}$. In the crystal state, all molecules are arranged in a crystalline structure, and in the isotropic state (liquid state) all molecules are not in any particular order. In figure 1, there is a visualization of the three states mentioned above.
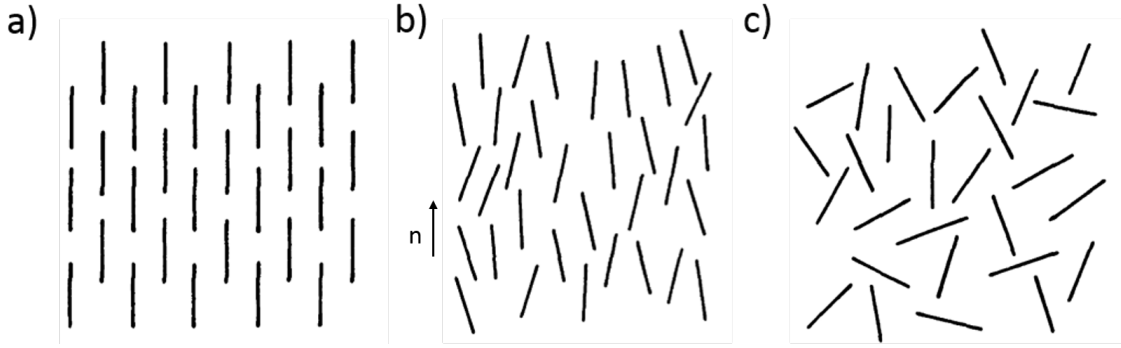
Figure 1: Molecular description for a) crystal, b) nematic, c) isotropic state [2].

This alignment creates an optically uniaxial specimen with strong birefringence [2]. In the nematic phase, molecules can flow internally but keeping the parallelism to the molecular director. Each molecule can be studied as a rod with cylindrical symmetry along the elongated axis.

The energy required to reorder the liquid crystal is so small that a slight perturbation, like a dust particle or a surface inhomogeneity, can change the entire liquid crystal structure. In order to describe the orientational order in the uniaxial case, we need the director $\vec{n}$ and the scalar parameter

$$S = \frac{1}{2} \left(\left\langle 3 \cos^2 \theta \right\rangle - 1 \right) \tag{1}$$

where θ is the angle that the molecular axis forms with the director and the brackets represent the average over the orientational distribution function [8]. For thermotropic liquid crystal, temperatures changes this parameter. For the isotropic liquid state, $S = 0$ and for the crystalline solid state, $S = 1$. In the case of uniaxial nematics, $S > 0.3$.

1.2 Anisotropies

Elongated shape of molecules of MBBA produce anisotropic physical properties. In general, measurements are taken parallel or perpendicular to the director $\vec{n}$. In this work, we study a system with convective instabilities of nematics under an oscillating electric field. For us, it is important to know the dielectric permittivity ε, the conductivity σ and the birefringence.

1.2.1 Dielectric anisotropy

The dielectric permittivity of the nematic liquid crystals is responsible for reordering of the molecules in response to an applied electric field. A dielectric anisotropy is defined when the values parallel $\varepsilon_{||}$ and perpendicular $\varepsilon_\perp$ to the director are different, therefore we write:

$$\varepsilon_a = \varepsilon_{||} - \varepsilon_\perp \tag{2}$$

We consider that nematic molecules carry a permanent dipole, therefore they can be orientated using electric fields. The value ε_a is positive if the permanent dipoles are parallel to the long molecular axis, which implies that the director orientates parallel to the electric field. It is negative when the permanent dipoles are perpendicular to the long molecular axis, which implies that the director orientates perpendicular to the electric field.

1.2.2 Conductive anisotropy

In the case of nematics, the conductivity is strongly dependent on the impurities and charge carriers. Nematics present conductive anisotropy when there is an anisotropy of mobility charges. It is defined as

$$\sigma_a = \sigma_{||} - \sigma_\perp \tag{3}$$

In general, the charge mobility of nematics are favored along the director, then $\sigma_a > 0$.

1.2.3 Birefringence

In nematics, visible light impinges on the liquid crystal and refracts in two different paths, which implies that there are two different refractive index. This is known as birefringence. Uniaxial nematics can be modeled by ellipsoids with cylindrical symmetry, therefore we define two axes according to both refracted light beams. We suppose that the incident light is linearly polarized, and take the long molecular axis as the optical axis. If the polarization is perpendicular to the optical axis, then light experiences the ordinary refractive index,

denoted as n_o. If the polarization is parallel to the optical axis, then light experiences the extraordinary refractive index, denoted as n_e.
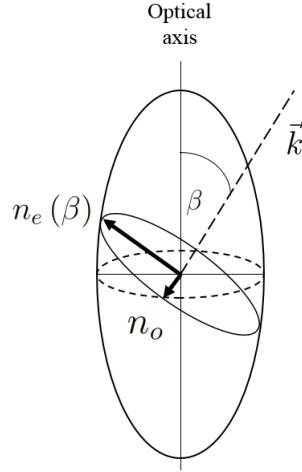
Figure 2: Birefringence in the refractive index ellipsoid [7] .

From this terms, we can write the birefringence as

$$n_a = n_e\left(\beta\right) - n_o \tag{4}$$

where β is the angle that forms the incident light $\vec{k}$ with the optical axis.

1.3 Electro-convective instabilities (Williams Domains)

Nematic liquid crystals present electro-hydrodynamic instabilities when they are under the application of an oscillating electric field at low frequencies. Even though the literature of instabilities is wide, we will describe only the case for instabilities produced for nematics with negative dielectric anisotropy , $\varepsilon_a < 0$, and positive conductive anisotropy, which is the case of MBBA [8]. We consider that the liquid crystal is inside a cell having a planar orientation, which is the case of this work. We consider that the incident light polarization is parallel to the molecular director, $\vec{n}$. In this configuration, the only refractive index is given by the extraordinary component, n_e.

In experiments, a low frequency voltage is applied to the liquid crystals. For low voltages the molecules remain aligned perpendicular to the electric field, as mentioned in section 1.2.1. At a voltage $V_{RMS} \sim 6$ $[V]$ the molecules reorder showing an unidirectional periodic pattern, for which the stripes formed are perpendicular to the director, $\vec{n}$. This pattern was first observed by Williams [11], therefore it is known as Williams domains.
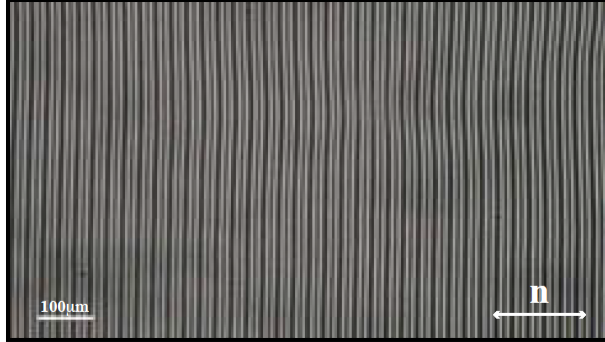
Figure 3: Williams domains in a cell of $2.9 \pm 0.5\,\mu m$ of thickness, at $V_{RMS} = 6.56$ $[V]$. Taken from [8] .

This periodical pattern is compared to an array of cylindrical lenses, that focus an incident plane wave in a series of lines (bright lines). It has been observed that Williams domains disappear when the incident light polarization is perpendicular to $\vec{n}$. In general, the periodicity of the pattern is the same as the sample thickness [8].

It has been observed that dust particles follow some particular motion inside the Williams domains. They exhibit circular flow lines as seen in convection, therefore Williams domains are called electro-convective instabilities [8]. As observed in figure 4, the circular flow will result in generating the cylindrical structure mentioned before. In Williams domains, not all molecules are parallel to the $\vec{n}$, but some are tilted with respect to the polarization. In this case, light experiences a combination of both, the extraordinary and ordinary refractive index. The effective index for this zones is always lower than n_e [8].
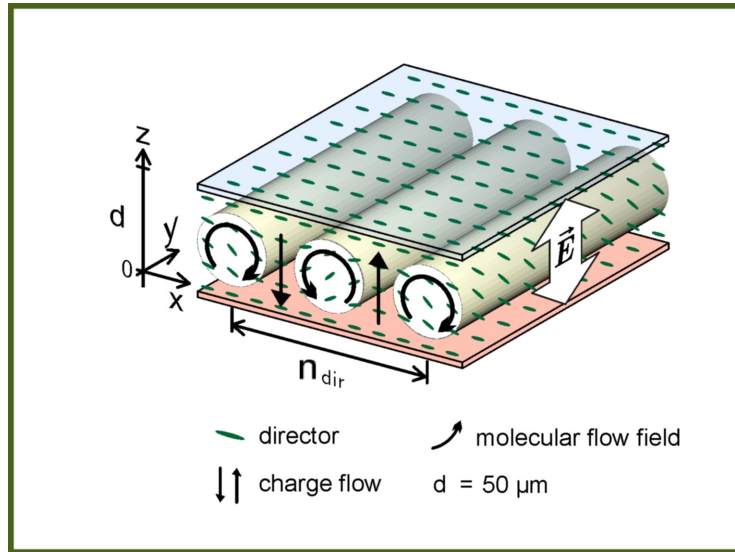
Figure 4: Illustration of the motion of molecules inside Williams domains. Taken from [5].

The Helfrich interpretation is used to explain the motion of molecules inside the Williams domains. In nematics, there are charge carriers as ions.
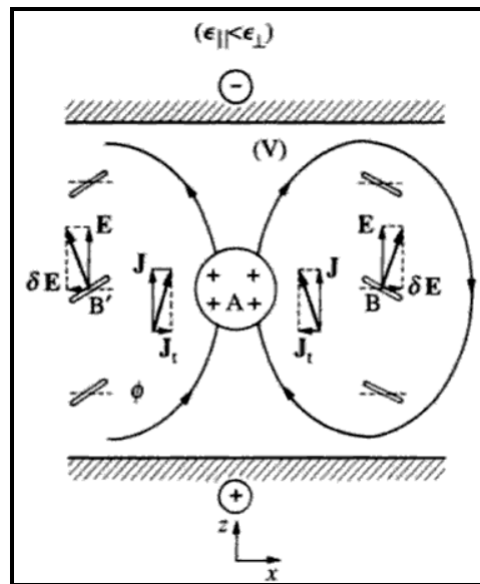
Figure 5: Helfrich interpretation of the motion of nematic molecules inside Williams domains. Taken from [3].

The main component of the current, $\vec{J}$ is parallel to the electric field, $\vec{E}$, but since $\sigma_a > 0$, there is a perpendicular component, $\vec{j}_t$. This produces an accumulation of positive charges

in point A. The electric field at point B is shifted by $\delta\vec{E}$. The initial distortion is produced by this electrostatic torque, because molecules tend to be orthogonal to the electric field.

The fluid around A experience a bulk force $q\vec{E}$, which generate a flow pattern qualitatively shown in figure 6. At point B, there is a strong hydrodynamic torque which tends to increase the distortion [3].

If the applied voltage is further increased, the periodic pattern generates dislocations or isolated defects, which look like a "fork". Later we will study how these defects generate optical vortices.

1.3.1   Dynamical scattering modes

As the applied voltage is increased, the number of defects from Williams Domains is also increased. The dislocations create a high scattering regime known as dynamical scattering modes. In the work of Pucci, two dynamical scattering modes are identified for MBBA, called DS1 and DS2 [8]. This regimes are characterized for the density of dislocations generated, but they are not the scope of this work.

2 Optical vortices

2.1 Physical background

Observations of light phenomena have motivated the discovery of new physical concepts. Johannes Kepler suggested that light has linear momentum because comet tails always point away from the sun [6]. After John Poynting developed the theory of electromagnetic pressure and momentum density and Albert Einstein showed that the motion of molecules in a radiation field is explained if each photon has a linear momentum of

$$\vec{p} = \hbar \vec{k} \tag{5}$$

where $\vec{k}$ is the wave vector, with $k = \frac{2\pi}{\lambda}$ and $\hbar$ is the Planck's constant. The concept of linear momentum of light has been exploited in several experiments, but in this work we convert this linear momentum of light into orbital angular momentum.

In order to understand optical vortices, we need to know what is the concept of spin angular momentum and orbital angular momentum. The total angular momentum of any light field is the sum of the spin and orbital terms.

2.1.1 Spin angular momentum (SAM)

Spin angular momentum is associated to circularly polarized light beams. Light has to be circularly polarized in order to have spin angular momentum [10]. For a single photon, spin angular momentum has a value of $\pm\hbar$.

2.1.2 Orbital angular momentum (OAM)

Orbital angular momentum is independent of the polarization state. It is associated to light beams with helical phase fronts, which have a phase singularity on the beam axis. This singularity has zero intensity on the beam axis, resulting in a ring shape for the intensity of

the light beam. For a single photon, the orbital angular momentum is:

$$L = m\hbar \tag{6}$$

where m is any integer number. In contrast to SAM, OAM can have infinite polarization states, depending on the value of m.

The most common helically phased beam are the Laguerre-Gaussian modes, which are used to illustrate intensity patterns of optical vortices.
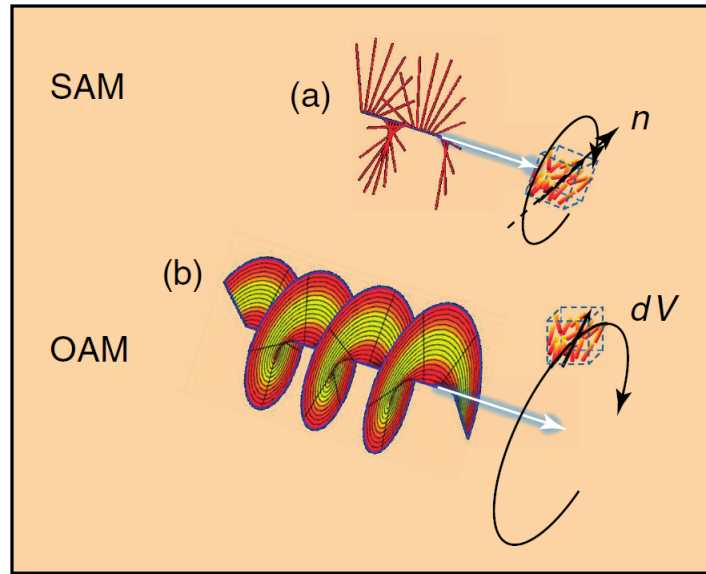
Figure 6: Comparison between spin angular momentum (SAM) and orbital angular momentum (OAM). (a) SAM induces a rotation to $\vec{n}$. (b) OAM induces a rotation motion of an element of volume around the light beam axis. Taken from [10].

2.2   Definition of optical vortices

An optical vortex is a point of zero intensity in a light field, which is associated to a helically phased beam. It is a phase dislocation, described by a number that is called topological charge, which is the number of twists the beam does in one wavelength. The topological charge m is an integer number, that can be positive or negative. Optical vortices always present orbital angular momentum.
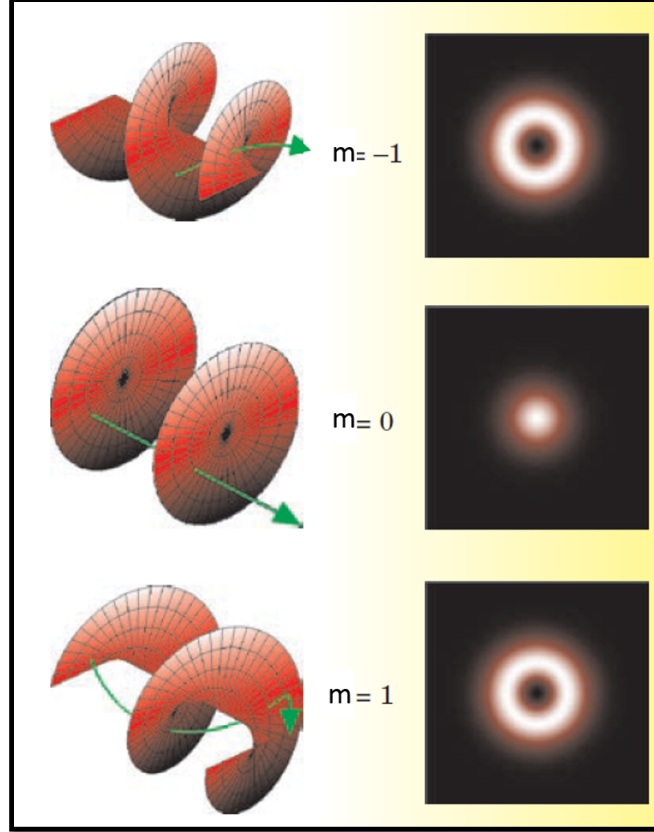
Figure 7: Optical vortices associated to each helically phased beam. The intensity pattern is a ring shape for $m = \pm 1$. Taken from [6].

2.3 How to generate optical vortices

We can simulate optical vortices of different topological charge by assuming that a periodical wave has a phase. For this purpose, we will use the "scalar field theory" and study the light behavior in presence of optical vortices. First, we want to generate the grating in the x-y plane. Consider that the periodical structure given by $\psi_1 = e^{ik_x x}$ for a wave traveling in the x-direction, where k_x is the wave vector. We need to add the phase given by $\psi_2 = e^{im\theta}$ where m is the topological charge of the optical vortex, also seen as the number of turns of the screw dislocation, and θ is the polar angle i.e. $\theta = \arctan\left(\frac{y}{x}\right)$. Then, the wave ψ that describes the grating with a vortex of topological charge m is, by superposition of $\psi_1 + \psi_2$:

$$\psi = e^{ik_x x} + e^{im\theta} \tag{7}$$

The intensity pattern H is given by the modulus squared of ψ, then:

$$H = \left| e^{ik_x x} + e^{im\theta} \right|^2 \tag{8}$$

which is simplified to:

$$H = 2\left[1 + \cos\left(k_x x - m\theta\right)\right] \tag{9}$$

As we are interested on the pattern, we will take $k_x = 2\pi$ considering $\lambda = 1$.

The diffraction pattern is obtained from the Fourier transform of H with a gaussian beam $\psi_G = e^{-(r/w)^2}$, where w is the width of the beam. In diffraction experiments, a laser beam has a gaussian intensity profile as ψ_G. The Fourier transform of $H\psi_G$ gives us the irradiance I, which is the diffraction intensity pattern of the grating H when impinged with a laser beam.

$$I = \mathcal{F}\left[H\psi_G\right] = \mathcal{F}\left[e^{-(r/w)^2}\left| e^{ik_x x} + e^{im\theta} \right|^2\right] \tag{10}$$

This Fourier transform is bidimensional, for the x-y plane it reads:

$$I = \int_{-\infty}^{\infty}\int_{-\infty}^{\infty} e^{-(r/w)^2}\left| e^{ik_x x} + e^{im\theta} \right|^2 e^{-i\,2\pi(ux+vy)}dx\,dy \tag{11}$$

The transformation has no analytical solution, therefore it was done numerically.

2.4 Computer simulations

2.4.1 Diffraction simulation

Taking the equations 9 and 10, we made the simulation using Matlab. The generated pattern shows a "fork" which is formed from two fringes converging into one. The simulation was done avoiding the singularity at zero, given by equation 9. The hologram mask generated shows incomplete fringes for high values of "y" along $x = 0$, but it does not change the diffraction pattern.
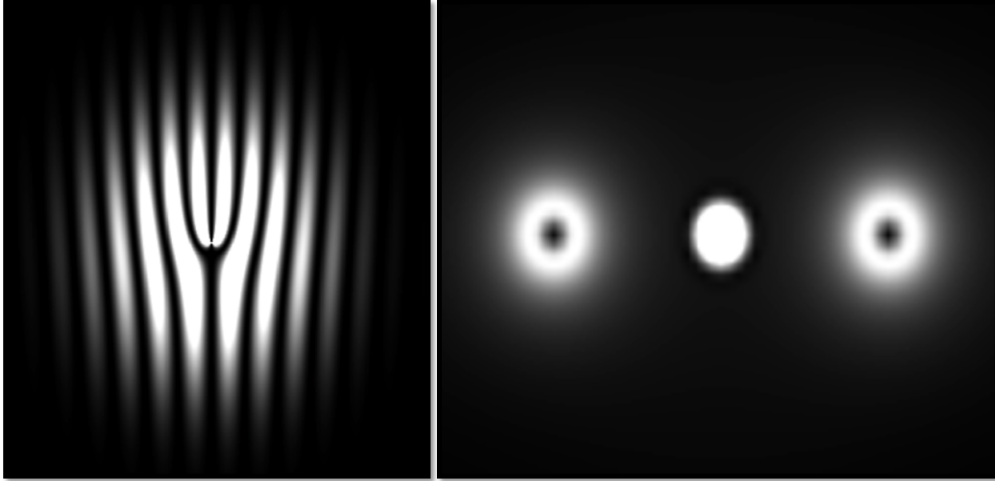
Figure 8: Self-made simulation of hologram with defect (left) and its diffraction pattern (right), using the Matlab code in section 7.1.

2.4.2 Interferometry simulation

When a plane wave is used as the reference beam, the interference pattern result in the reconstruction of the "fork" shape of the hologram. This is produced because of constructive interference of light with the Williams domains.
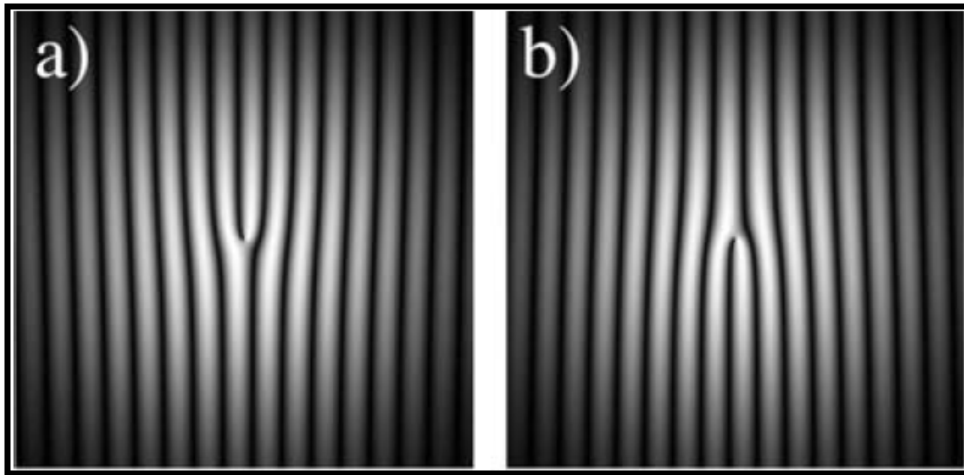
Figure 9: Interference pattern for a plane wave front, (a) $m = 1$ and (b) $m = -1$. Taken from [1].

When a spherical wave is used as the reference beam, the interference pattern result in a spiral-like shape, which shows a handedness according to the order of the diffracted beam.

This is produced by the intersection of the helical beam with a spherical wave, centered on the beam axis.
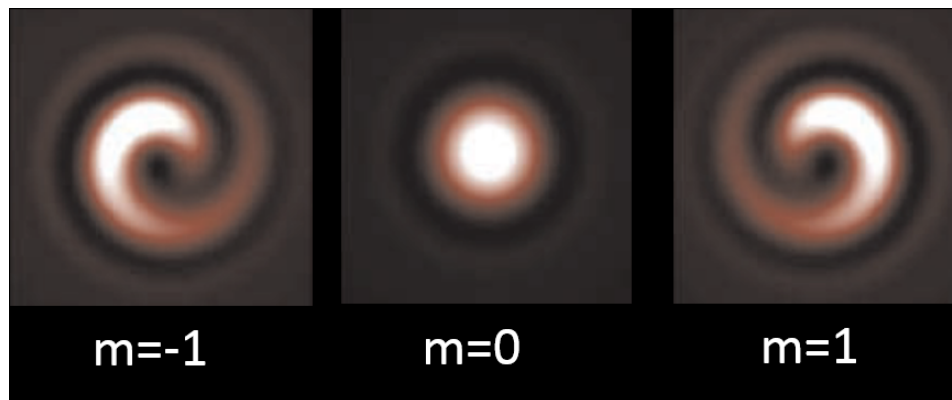
Figure 10: Interference pattern for a spherical wave front. Taken from [6].

2.5   Applications

A light beam carrying angular momentum can interact with matter and transfer this angular momentum to objects [10]. Therefore, optical vortices can be used to trap neutral particles, which are known as optical tweezers. In this case, neutral particles are affected by the angular momentum given by the defect [1].

The holographic mask can have different designs, but the diffraction pattern is unique and can be used to focus celestial objects in telescopes. Many physical experiments, like Kelvin-Helmholtz instabilities may be studied using this optical system [1].

3   Experimental measurements

3.1   Liquid crystal cell fabrication

The liquid crystal used in this work is MBBA, without any solvent or micro-particles. MBBA is generally stored in refrigeration, for which it is in solid state, looking like a yellowish crystal. The cell itself consists of two parallel glass slides separated by plastic pieces.
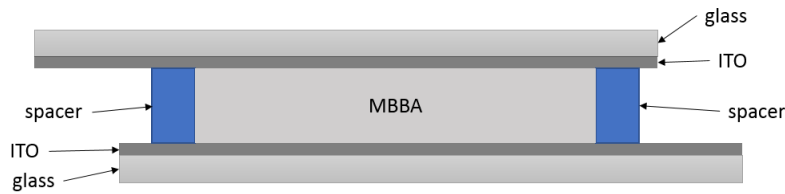
Figure 11: Liquid crystal cell scheme, not to scale.

This cell has two openings that are used to fill the internal cavity with liquid crystals. The surfaces facing the cavity are previously painted with ITO (Indium Tin Oxide) which is a transparent conductive paint layer, resulting in a capacitor-like cell which allows the study of optical phenomena of liquid crystals under the application of an electric field. These surfaces are slightly rubbed along a unique direction for both surfaces, for this reason the molecular director $\vec{n}$ is known to align in this direction.
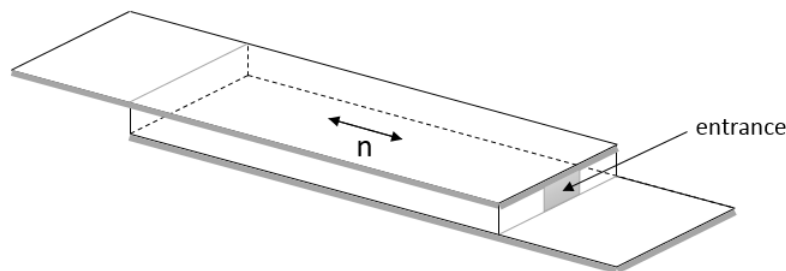
Figure 12: Molecular director $\vec{n}$ alignment with the cell.

The effective electrode area of ITO is 1 cm^2, which is enough to observe several defects in Williams Domains.

It is recommended to make the electrical contacts, soldering wires to each glass slide, before filling the liquid crystal inside the cell. This is to avoid any dust particle from soldering to get into the the liquid crystal. MBBA has to be heated up to 70 °C, to be in the isotropic liquid state. The filling of the liquid crystal happens due to surface tension at 70 °C, for which it flows from one opening to the other, following the molecular director direction. MBBA is transparent to visible light at room temperature. Even though this cell fabrication was done in a clean room, some impurities were observed in the cell. This impurities did not change the correct behavior of the cell nor made an electrical shortcut.

MBBA has the following physical properties, mentioned in section 1.2. It has a negative dielectric anisotropy $\varepsilon_a = -0.53$ and positive conductive anisotropy $\frac{\sigma_{\parallel}}{\sigma_{\perp}} = 1.5$ at 25 °C. In particular, for MBBA the molecular director can be taken in direction parallel to the preferred alignment direction, because of the symmetry of the molecules of MBBA. The chemical structure of MBBA is N-(p-methoxybenzylidene)-p-butylaniline.
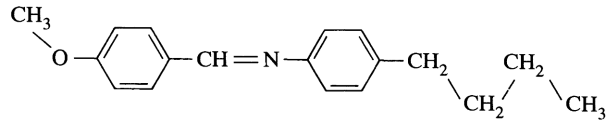
Figure 13: Chemical structure of MBBA. Taken from [3].

MBBA is known to be in the nematic phase from 20 °C to 47 °C , therefore is has been widely used for laboratory experiments [3].

3.2   Microscope observation

In order to observe the William Domains, we need to use a microscope setup with polarized incident light. For this work, we used two microscopes for different purposes of the experiment. The first stage consisted on the identification of the reaction of MBBA to different

values of field and frequency. The second stage consisted on the localization of defects once the cell was placed in the optical table, in the diffraction and interferometry experiments, which will be later discussed.

For the identification of optical properties of MBBA under the application of an electric field, we used a classical desktop microscope. This microscope has an incorporated CCD camera that stores images in high definition for several amplifications. We applied a sinusoidal voltage from a function generator, which was connected to an amplifier to achieve higher amplitudes. In this sense, we are interested in the root mean square voltage, which for a sinusoidal wave is

$$V_{RMS} = \frac{V_{pp}}{2\sqrt{2}} \tag{12}$$

where V_{pp} is the voltage peak to peak. This measurement was taken for the high impedance configuration of the multimeter.

The first observations showed the expected behavior of the formation of periodical fringes. Additionally, the different regimes mentioned in section 1.3.1 were observed by changing the amplitude of the applied voltage.
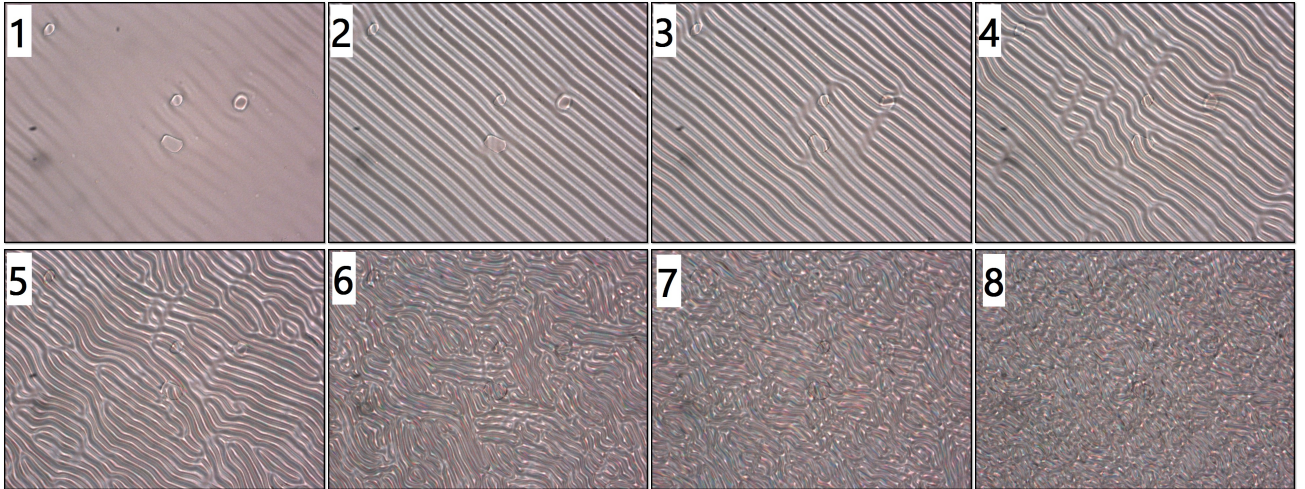
Figure 14: Transition to dynamical scattering mode of MBBA. Voltages values are: 1) 5.91 [V], 2) 6.17 [V], 3) 6.54 [V], 4) 7.06 [V], 5) 7.73 [V], 6) 10.18 [V], 7) 11.39 [V], 8) 14.34 [V] at a fixed frequency of 10 Hz. Cell spacing is 25 μm.

We were interested in studying the defects formed in the Williams Domains, therefore it

is convenient to get voltage values at which defects are stable for some minutes. Under the microscope, it was evident that defects were flowing slowly through the fringes.
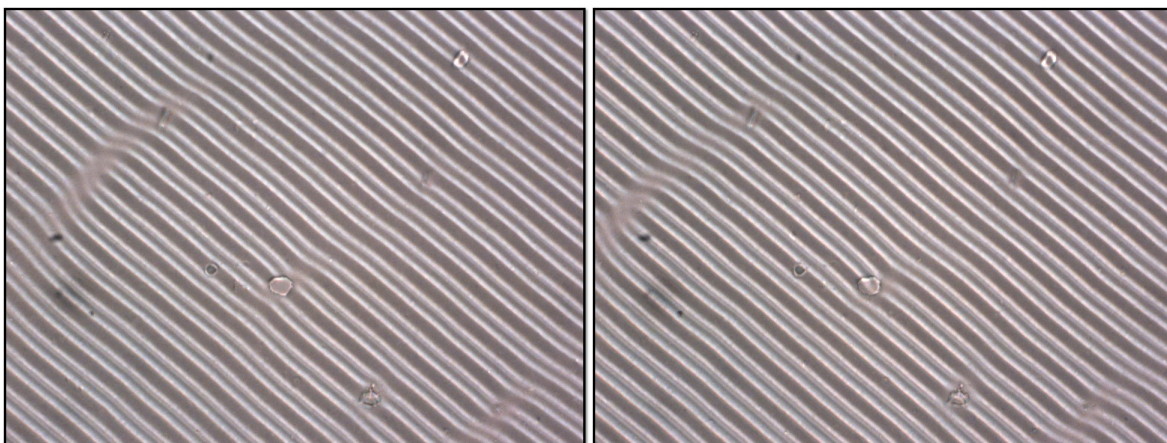
Figure 15: Single charge defect moving left. Cell spacing is 25 μm.

Two cells with nominal spacing of 25 μm and 50 μm were used. For each cell, the Williams Domains periodicity is approximately equal to its cell nominal separation. For the 50 μm cell, defects were more static for several minutes. For this reason, we used this cell for the diffraction and interferometry experiments.

The defect formation has a "fork" shape, which is seen as one fringe dividing into two fringes. This is known as a single charged defect, or a defect with topological charge $m = \pm 1$.
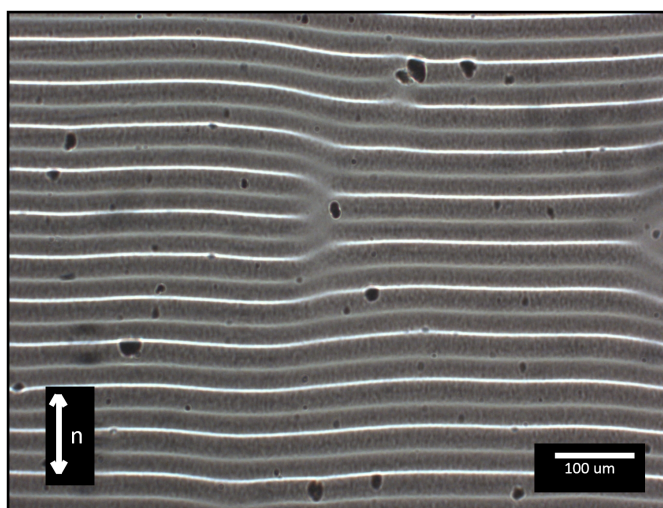
Figure 16: Single charged defect. Cell spacing is 50 μm.

The second microscope showed the same fringes and defects as seen in the desktop microscope. This microscope was a USB portable microscope which was useful because it could be aligned with the laser in order to center the defect.
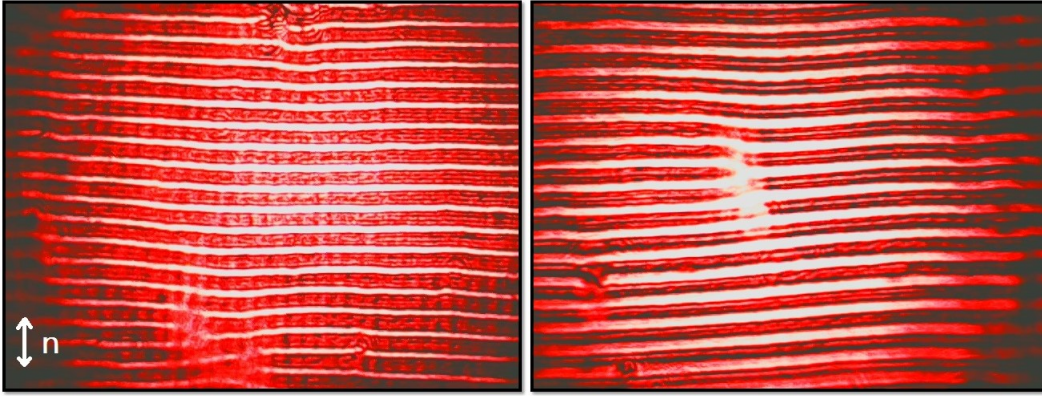
Figure 17: William Domains seen from USB microscope, without defects (left) and with a single defect (right), for $V_{RMS} = 7.01$ $[V]$. Cell spacing is 50 μm.

3.3   Diffraction and interferometry setup

The setup consisted on several optical elements connected to an optical table. The optical table is the key of every optical experiment because it reduces vibrations and also keeps optical elements fixed at a given position. The setup for the diffraction and interferometry experiment is the same. We attached the following elements to the optical table: a He-Ne laser, two beam splitters (BS1, BS2), two mirrors (M1, M2), two linear polarizers (P1, P2), two half-wave plate, a CCD beam profiler, a lens ($f = 5cm$), the USB microscope and the sample.

In principle, the laser would split in two similar phase laser beams at BS1. Then the two beams would be passed through the set $\frac{\lambda}{2}$-polarizer, which basically guarantees that light will be linearly polarized (Refer to section 7.2 for more information about the $\frac{\lambda}{2}$ wave plate). When light passes through the $\frac{\lambda}{2}$ wave plate, it linearly polarizes along a unique direction without changing the initial light intensity. The polarization was taken perpendicular to the optical table. The two beams have the same properties after P1 and P2.

For the diffraction experiment we blocked the beam after P1, taking only the beam impinging the sample. The USB microscope was placed after the sample, and only used to localize the defects and align them to the laser beam. The intensity patterns from the diffraction was taken with the CCD beam profiler. The sample was placed making the director $\vec{n}$ parallel to the polarization of the beams. Williams domains are perpendicular to $\vec{n}$, which means that they are parallel to the optical table.

For the interferometry experiment we do not block the beam after P1, so that light passes through the lens. This beam is magnified and has a spherical wave front at the focal distance. This beam has to be aligned with the diffraction orders at BS2 by tilting M2. The angle of diffraction obeys Bragg's law:

$$d \sin \theta_m = m\lambda \tag{13}$$

where $d = 50\mu m$ for the 50 microns sample, and m is the order of the diffracted beams. For this work we analyzed the cases of $m = \pm 1$.

For both experiments, the sample was firmly attached to a heavy holder that allowed us to move the sample by microns. This was useful to find zones of the Williams Domains with and without defects. Also, the sample was connected to the wave function generator which applied a voltage at $70\ Hz$. Since function generators do not get voltage values higher than $V_{RMS} = 3\ [V]$, then we connected it to an amplifier to achieve $V_{RMS} \sim 7\ [V]$.

For this work, it was important to have every element correctly aligned. In particular, the laser beams had to be aligned in all the setup, parallel to the optical table. We used a pinhole to verify the alignment in the setup.
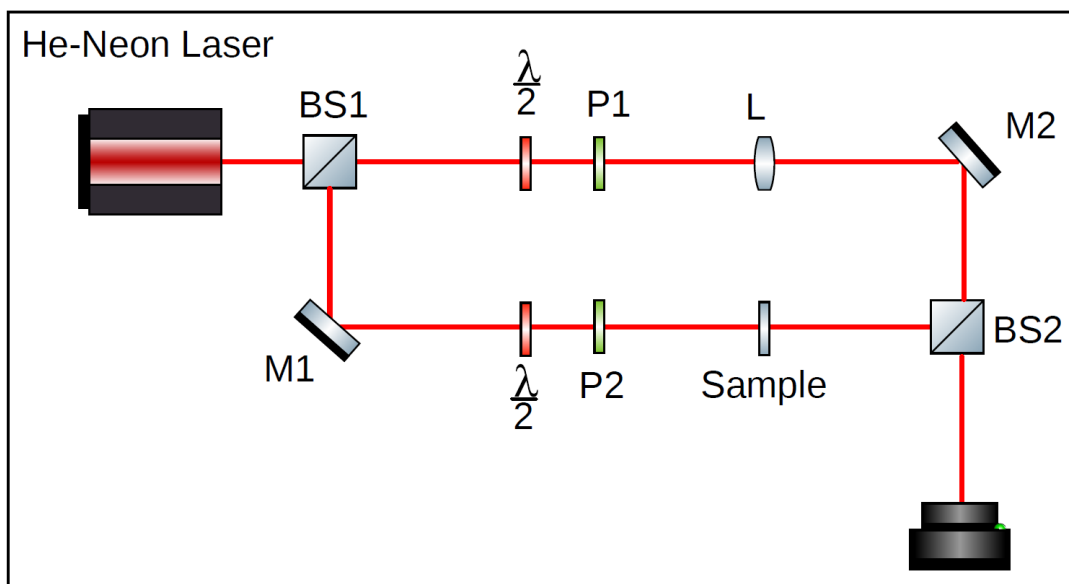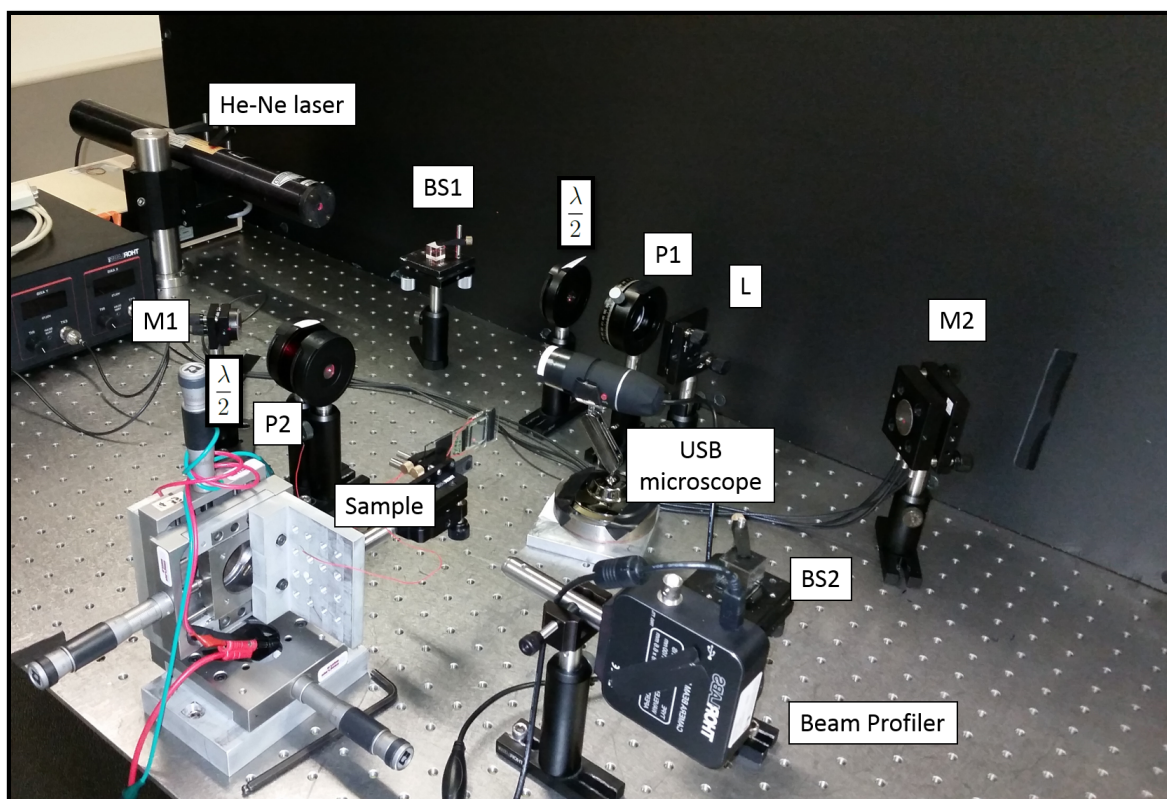
Figure 18: Experimental schematic setup.

Figure 19: Picture of the experimental setup.

3.4 Results discussion

The results of the diffraction and interferometry experiments are summarized in figure 20. This figure also contains some intensity patterns that occur when there is no electric field applied to the sample.

In (a) we observe the incident beam, which has a symmetric gaussian profile. For (b) we observe the transmission of the incident beam through the liquid crystal in the nematic phase. The pattern still holds the gaussian profile, but it is not symmetric due to internal motion of molecules in the cell. As mentioned before, at room temperature and no applied field, MBBA molecules tend to align along the molecular director, $\vec{n}$. Some of this molecules are not perfectly aligned to $\vec{n}$, so that there is a distortion of the incident beam.

In (c) we show the interference pattern between the incident beam and the spherical wave coming out from the lens. We observe a gaussian profile at the center, surrounded by circular fringes, which is a feature of interference of Michelson's experiment [4]. In (d) we show the interference pattern between the spherical wave and the beam coming out from the liquid crystal cell. Once again there is a distortion in the intensity pattern due to internal motion of molecules in the cell.

In (e) we observe the diffraction pattern produced by Williams domains of MBBA without any defect. The first diffracted orders corresponding to $m = 1$ and $m = -1$ are equally spaced, according to equation 13. The transmitted beam keeps a symmetrical shape once the electric field is applied, in contrast to (b). The diffracted beams also have a gaussian profile, but with less intensity than the transmitted beam.

In (f) we observe the interference pattern of the diffraction seen in (e), when the spherical wave is centered in the transmitted beam, $m = 0$. We notice that the interference pattern of the transmitted beam is similar to (c). For the diffracted beams, the tail of the reference beam has a plane wave front, which results in the reconstruction of the Williams domains.

In (g) and (h) we observe the interference pattern of the diffraction centered at the diffracted beams. For these cases, the beam has the same physical properties as the transmit-

ted beam, which are the phase and the gaussian intensity profile. Therefore, the interference pattern at the diffracted beams is similar to (c).

In (i) we observe the diffraction pattern produced by a single charged defect in Williams domains. In this case, the transmitted beam is not changed as in (e), but the first diffracted orders have a ring-like intensity profile. This profile correspond to an optical vortex. We also observe that the diffracted beams have similar intensity profiles. In (l) we observe the interference of the diffracted optical vortices with a plane wave. As a result, we obtained the reconstruction of the Williams domains with only single charged defect for each diffracted beam. The defect has the "fork" shape mentioned in section 2.3. For (m) we observe the interference pattern of the diffraction of (i) with a spherical wave centered at $m = 1$. The resultant pattern is the spiral shape, which opens clockwise. This was the expected result as mentioned in section 2.4.2. The transmitted beam does not change, and is equivalent to (g). The other diffraction order is far from the spherical wave tail, but a closer look would reveal that it shows the fork defect, as for (l). For (n) we observe the interference pattern of the diffraction of (i) with a spherical wave centered at $m = -1$. The resultant pattern is the spiral shape, which opens counter-clockwise. The transmitted beam does not change, and is equivalent to (h). The other diffraction order is far from the spherical wave tail, but a closer look would reveal that it shows the fork defect, as for (l).

From (m) and (n) we can identify that there is a conservation of orbital angular momentum given by the opposite handedness at the diffraction orders $m = -1$ and $m = 1$.
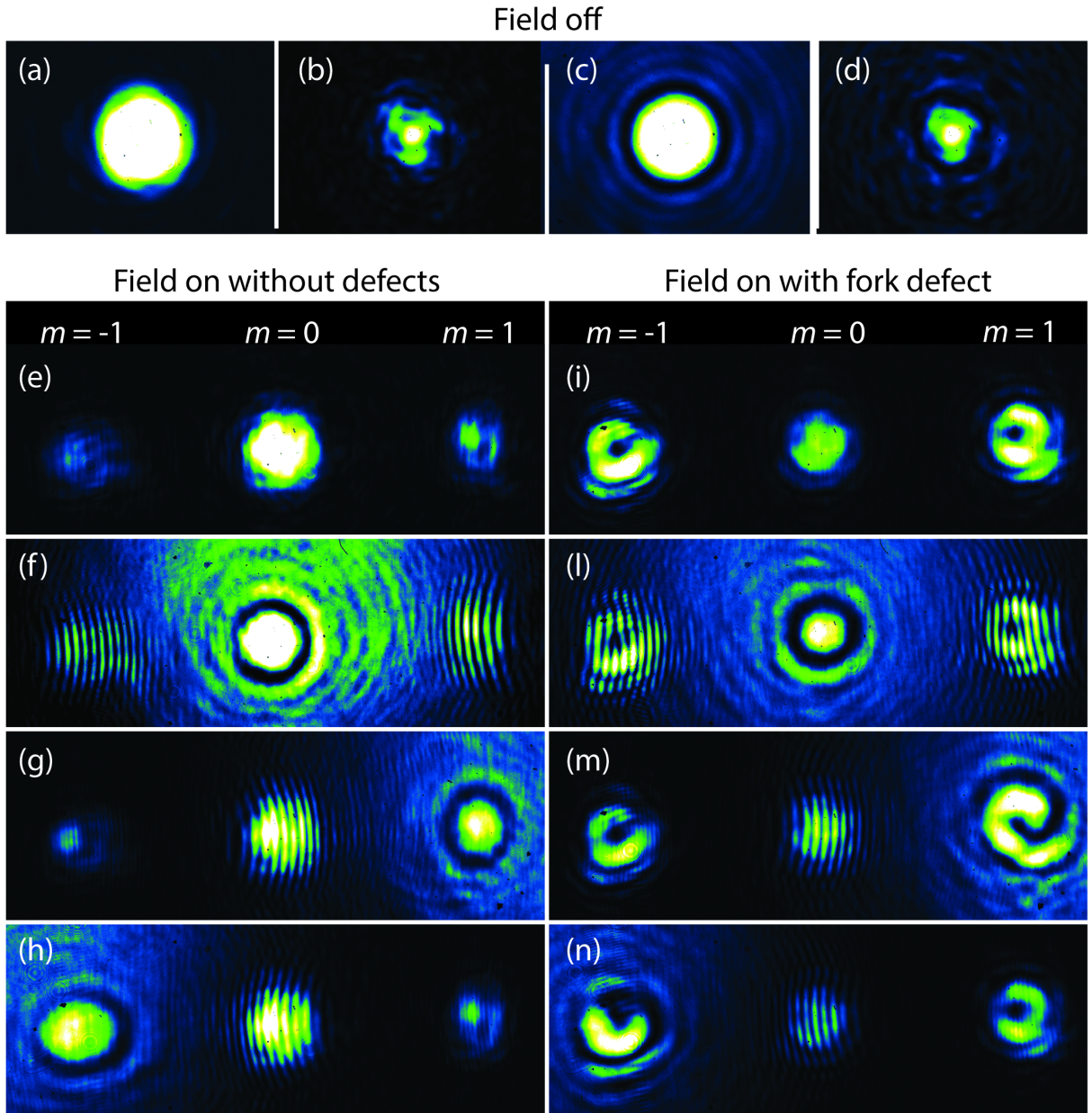
Figure 20: (a) Incident beam. (b) Beam transmitted through the LC cell for $V = 0$, i.e. in the absence of Williams Domains. (c) Interference between the incident beam and a spherical wave. (d) Interference between the zero-voltage transmitted field and spherical wave. (e) Transmission through an array of the Williams Domains obtained for $V_{RMS} = 6.81\,[V]$ at $f = 70\,[Hz]$ showing the direct beam ($m = 0$) and first diffraction orders ($m = \pm1$). (f,g,h) Interference of the transmitted field with a spherical wave aligned with the beam of order $m = 0, 1, -1$, respectively. (i-n) Transmitted field in the presence of a fork defect obtained for the same conditions as in images (e-h).

4   Future measurements and recommendations

Higher orders could be studied by tilting M2 as for the interferometry experiment in figure 18. Briefly, we obtained the intensity pattern of orders $m = 1, 2, 3$ for diffraction and interferometry.
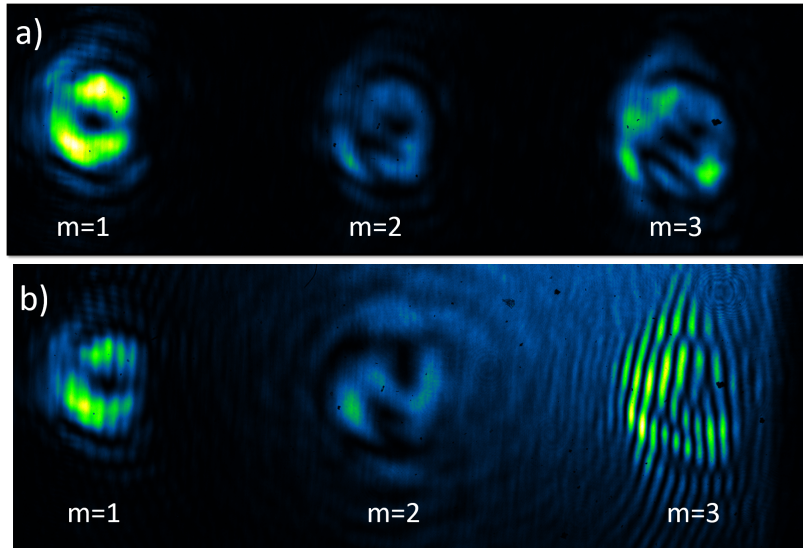

Figure 21: a) Diffraction intensity pattern for $m = 1, 2, 3$. b) Higher order interferometry, spherical wave centered at $m = 2$, plane wave for $m = 1$ and $m = 3$.

The spiral behavior of light interferometry for $m = 2$ is as expected. The interferometry pattern of $m = 3$ shows three single charged defects tilted with respect to the diffraction direction. This effect is purely produced by the diffraction and has no relation to the spherical wave front coming from the lens. This tilting effect is mentioned by Carpentier et.al. as a change in phase from the reference beam[1].

Other experiment could be adding micro-particles to the sample to get a localized defects, because in a pure MBBA sample cell the generation of single charged defects is spontaneous. In this work, there is no method to find where the defects would appear before the electric field is applied. After the electric field is applied, direct observation was needed to find the defects in the sample.

As a recommendation, it is important to keep the laser beam aligned in all the setup.

Also, check that the MBBA still works as expected, because a sudden voltage shock could damage its structure and generate bubbles. Despite the MBBA is damaged, it does not change its structure under the application of an electric field.

5   Conclusions

We performed experiments of interferometry that allowed us to find the angular momentum of the light. We found that MBBA creates very stable Williams domains for an applied voltage of $V_{RMS} = 6.81\,[V]$, for which we observed several "fork" shaped defects, with single topological charge. For a plane wave, the interferometry pattern reconstructs the "fork" shape defect, which reveals the topological charge of the defect. For a spherical wave, the interferometry patterns centered at the diffracted beam gave us the order of diffraction, just by looking at the handedness of the spiral shape. The interference patterns give visual information of the phase, because of the constructive interference of light, and confirm the helicity of the diffracted beams. The conservation of orbital angular momentum was confirmed when the spirals showed opposite handedness for the first order diffracted beams. Initially the first order diffraction was studied, but this work could be extended for higher orders.

6 References

References

[1] Carpentier, A., Michinel, H., Salgueiro, J and Olivieri, D. (2008). *Making optical vortices with computer-generated holograms.* DOI: 10.1119/1.2955792

[2] Chandrasekhar, S. (1992). *Liquid Crystals.* Cambridge: Cambridge University Press.

[3] De Gennes, P. and Prost, J. (1993). *The Physics of Liquid Crystals.* Oxford Science Publications, 1993.

[4] Hecht, E. (2002). *Optics.* Reading, MA: Addison-Wesley.

[5] Heuer, J. (2007). *Electroconvection: Pattern formation in liquid crystals.* Retrieved from http://www.uni-magdeburg.de/anp/projects/pattern_form/index.htm

[6] Padgett, M., Courtial, J., & Allen, L. (2004). *Light's Orbital Angular Momentum.* Physics Today, 57(5), 35-40. doi:10.1063/1.1768672

[7] Peatross, J., & Ware, M. (2015). *Physics of light and optics.* Provo, UT: Brigham Young University, Department of Physics.

[8] Pucci, G. (2011). *Two phenomena of self-adaptation in out-of-equilibrium systems* (Doctoral thesis. Université de Paris VII).

[9] Thorlabs. (2017). *Mounted Zero-Order Half-Wave Plates.* Retrieved from https://www.thorlabs.com/newgrouppage9.cfm?objectgroup_id=711

[10] Torres, J. P., & Torner, L. (2011). *Twisted photons applications of light with orbital angular momentum.* Weinheim: Wiley-VCH.

[11] Williams, R. (1963). *Domains in liquid crystals.* Journal of Chemical Physics, 39:384.

7 Annexes

7.1 Matlab code for the diffraction of optical vortices using a plane wave

% Matlab model simulation of the diffraction of optical vortices

```
clc; clear;
Username='Juan Pablo Yunda';
% Variable inizialization
Lambda = 10; LScreen=10; m=2; k = 2*pi; w=3;
% gridspacing definition
yMax = LScreen; % set limits
xMax = yMax; % for the screen
Nx = 1000; Ny = 1000; % number of points in x, y
x = linspace(-xMax,xMax,Nx); y = linspace(-yMax,yMax,Ny);
% loop for the calculation of the hologram with defects of charge m
fGH=zeros(100,100);
for i=1:Nx
    for j=1:Ny % Gaussian beam "fi_G" multiplied by the hologram H
        fGH(i,j)=exp(-(x(j)^2+y(i)^2)/w^2)*(2+ 2*cos(k*x(j)-m*atan(y(i)/x(j))));
    end
end
% Here we convert this matrix to the reciprocal space, by using fft2()
% which gives a complex matrix.
Intensidad = fft2(double(fGH)) ;
% Here we take the absolute value of this complex matrix to be able of
% making a plot. fftshift reorders the matrix, making zero phase coincide
% at the origin. Otherwise, same phase points, 0 and +-2*pi are at the
% corners of the graph
IntensidadModulo = abs ( fftshift(Intensidad) );
% take a submatrix to interpolate for a better plot
ModuloGraph = IntensidadModulo((420):(580),(420):(580));
%Make the interpolation of this matrix before plot
ModuloGraph = interp2(ModuloGraph,5);
% Plotting parameters
clf; figure(gcf); % Cleans "figure"; opens window "figure"
NGrayLevels = 255; % Number of gray levels
% graph 1
subplot(1,2,1); Iimag=imag(abs(fGH)); % Here the intensity is adjusted
IntenGray = (fGH/2.0) * NGrayLevels;
image(x,y,IntenGray); % Make the plot
colormap(gray(NGrayLevels)); % uses plot in grayscale
```

```
xlabel('x (m)'); ylabel('y (m)');
title([Username,' ,',date,', ','Simulation of the hologram mask with defect']);
%
subplot(1,2,2);
IntenGray = (ModuloGraph/100.0);
image(x,y,IntenGray); % make the plot
colormap(gray(200)); % uses plot in grayscale
xlabel('x (m)'); ylabel('y (m)');
title([Username,' ,',date,', ','Simulation of the diffraction given by the mask']);
```

7.2 Half-wave plate operation principle

Wave plates are also known as retarders. They are usually made of birefringent materials, and are used to change the polarization of a light beam by 2θ, where θ is the angle in polarization of the light beam with the optical axis of the wave plate [4]. In other words, if the incident light is linearly polarized at $\theta = 0°$, then placing the optical axis of the half-wave plate at 45° would generate an output light beam linearly polarized at $\theta = 90°$.
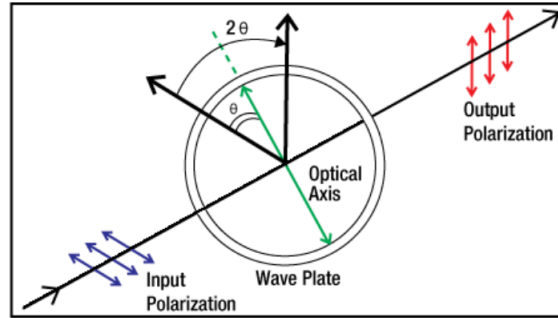

Figure 22: Half-wave plate change in polarization. Taken from [9].

The configuration of $\frac{\lambda}{2}$ wave plate and linear polarizer, as on figure 18, generate the following intensity pattern:
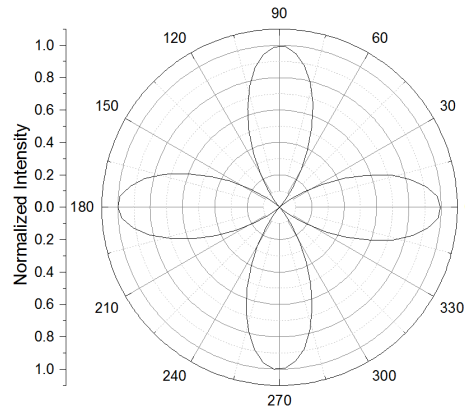

Figure 23: Polar plot of the intensity of the set half-wave plate and linear polarizer. The angle is the phase between the half-wave plate and the polarizer.

Here the incident beam passed through the $\frac{\lambda}{2}$ wave plate fixed perpendicular to the optical table, and then the polarizer angle was changed. The polar plot shows the intensity of the transmitted beam, generating four maxima when the linear polarizer is parallel to the $\frac{\lambda}{2}$ wave plate. The beam that comes after this configuration is linearly polarized.